Probing the Complexity of the Infall Envelope around the W3(OH) Massive Star-Forming Region

Wei-Ting Kuo and Vivien Chen
Department of Physics and Institute of Astronomy, National Tsing Hua University

Abstract

We have observed emissions of HCO^+ (1-0), $C^{18}O$ (1-0), and N_2H^+ (1-0) toward the W3(OH) massive star-forming region, which is in the course of developing a small OB stellar group, including an ultra-compact HII region,W3(OH), and at least six more HII regions. The HCO^+ (1-0) spectra show the blue-skewed infall asymmetry in the circumcluster envelope, suggesting a large-scale ongoing collapse over 50" (0.4 pc). The $C^{18}O$ (1-0) emission shows a velocity gradient (0.13 kms^{-1} $arcsec^{-1}$) across the W3(OH) region, proposing possible rotation motions over 30" (0.24 pc). The N_2H^+ (1-0) emission traces dense and quiescent gas in two filaments. As a first step to describe the infall motions, we utilize RATRAN (Hogerheijde & van der Tak 2000) to analyze our HCO^+(1-0) data cube. For the rotation motions, we present a position-velocity diagram and our preliminary estimate gives that the specific angular momentum at 0.06 pc is 0.17 kms^{-1} pc (3.51 x 10^4 kms^{-1} AU).

Introduction

The vicinity of the ultracompact (UC) HII region W3(OH) is a nearby (1.67 kpc; Matsumoto et al. 2011) massive star-forming region, containing at least seven HII regions within an extent of 40″ (circles; Harten 1976). Here, we present full-synthesis HCO^+ (1-0), $C^{18}O$ (1-0), and N_2H^+ (1-0) imaging around W3(OH) with a high spatial resolution by combining the Berkeley-Illinois-Maryland Association (BIMA) Millimeter Array and the Arizona Radio Observatory (ARO) 12m Telescope data.

	HCO^+ (1-0)	$C^{18}O$ (1-0)	N_2H^+ (1-0)
configuration	BIMA C,D + ARO	BIMA B,C,D + ARO	BIMA B,C,D + ARO
resolution	6.3"	4.0"	5.0"

Result

HCO^+ (1-0)

The spectrum around W3(OH) (red line in Fig. 1a) shows a stronger blue-shifted peak at -49.5 kms^{-1} and a red-shifted peak at -44.5 kms^{-1}. This blue-skewed line profile is often used to identify infall candidates (Evans 1999). In the presence of infall motions, the foreside of the envelope is redshifted while the backside is blue-shifted (Fig 1b; Zhou & Evans 1994). In the red-shifted foreside, the emission from the hotter central region is partially absorbed by the outer region at lower temperature. In the blue-shifted backside, the emission arrives at the observer without much absorption.

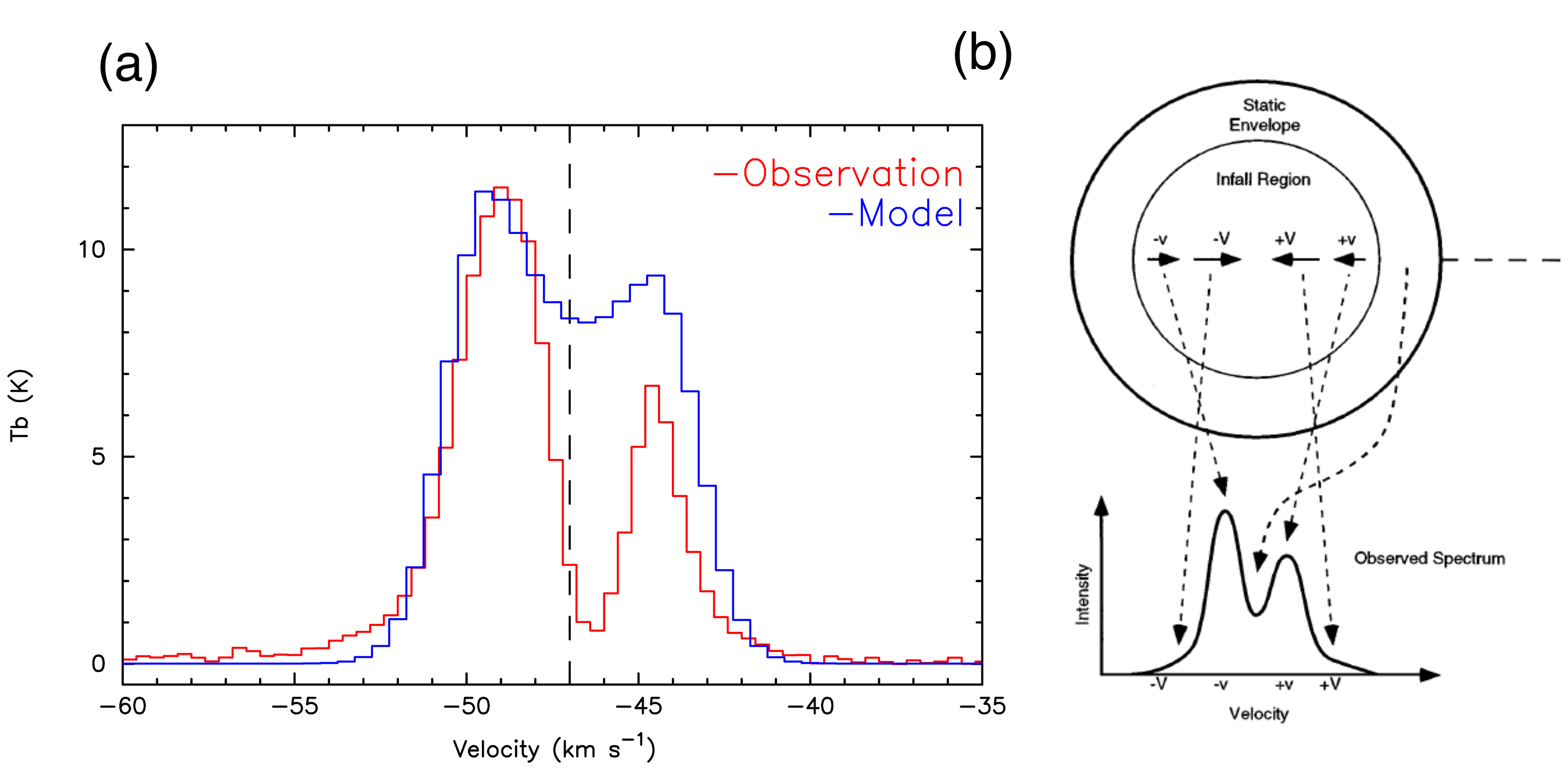

Fig. 1. - (a) The spectrum in the central rectangle with dimension 20"x20"(red line) and the best fitting spectrum of our model (blue line)
(b) The line profile an inside-out collapse model (Evans 1999)

N_2H^+ (1-0)

The integrated intensity map of N_2H^+ (1-0) (Fig. 2) shows two filamentary structures. The north-south filament is more elongated and compact than the east-west filament, which is similar with that observed in NH_3 (1,1) (Wilson et al. 1993). In the vicinity of HII regions (circles; Harten 1976), N_2H^+ (1-0) tends to be destroyed due to sublimation of CO. Except in light blue circle, strong emission of N_2H^+ is detected, suggesting the existence of a dense massive clump for further star formation.

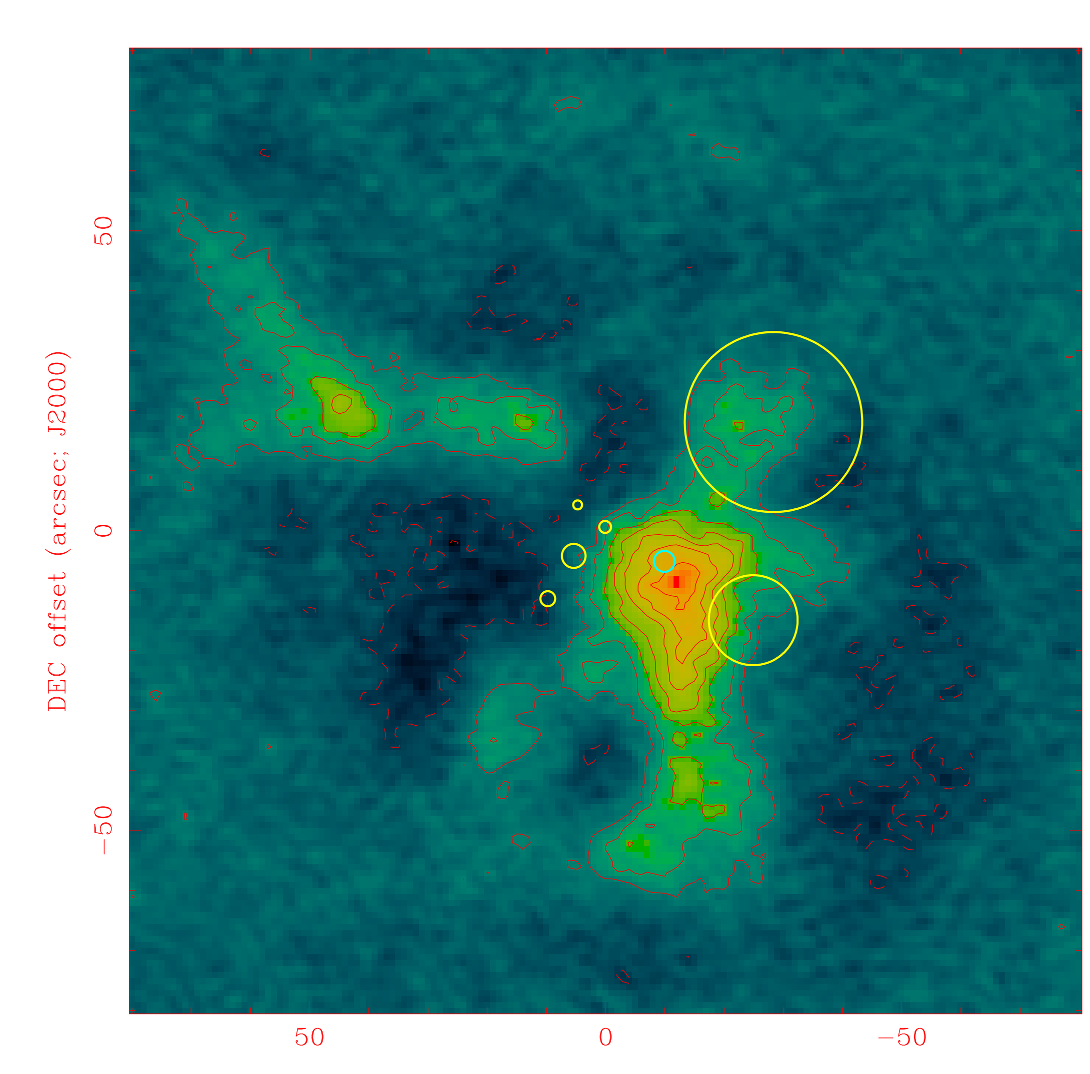

Fig. 2. The Integrated map of N_2H^+(1-0)

$C^{18}O$ (1-0)

The $C^{18}O$ (1-0) channel map (Fig. 3) shows that the emission peak shifts (~8") from the east to the south of W3(OH) (central circle) as velocity increases from -49.5 to -45.9 kms^{-1}. This shift may represent the existence of a large velocity gradient. From the velocity-weighted map (Fig. 4), this velocity gradient is about 0.13 kms^{-1} $arcsec^{-1}$, corresponding to 16.5 kms^{-1} pc^{-1}, suggesting possible rotation motions. For further study of these rotation motions, we derive a position-velocity (PV) diagram from a cut along the axis at position angle 47° (Fig. 5). We assume that this rotation axis is parallel to the line of sight, and the angular rotation velocity derived from the slope of Figure 5 is 1.42 x 10^{-12} $rads^{-1}$. Meanwhile, Figure 5 shows the range of these rotation motions is within 40" (0.32 pc), and the rotation velocity and the specific angular momentum are estimated to be 2.84 kms^{-1} and 0.17 kms^{-1} pc (3.51 x 10^4 kms^{-1} AU) at a radius of 0.06 pc.

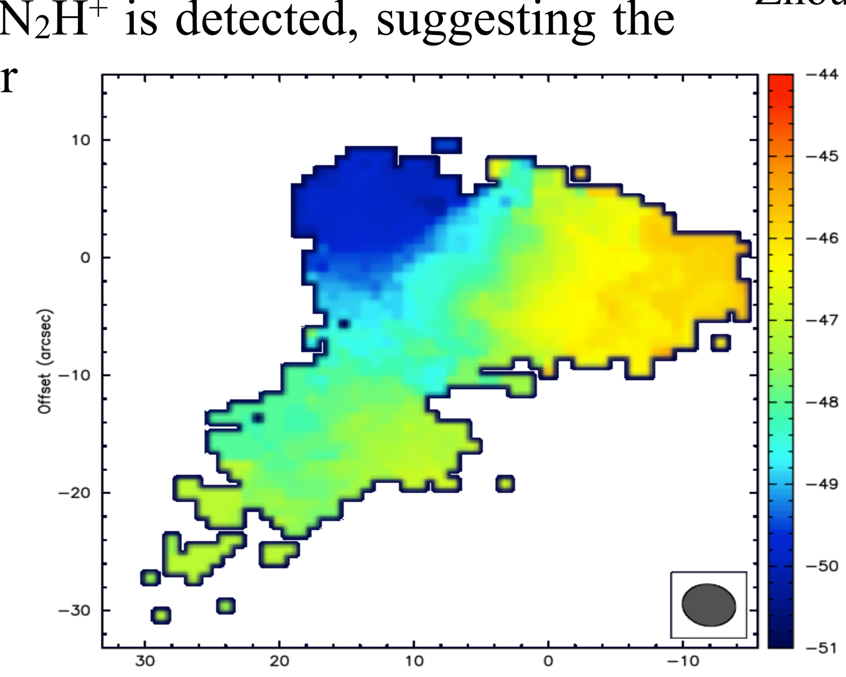

Fig. 4. The $C^{18}O$ (1-0) velocity-weighted map

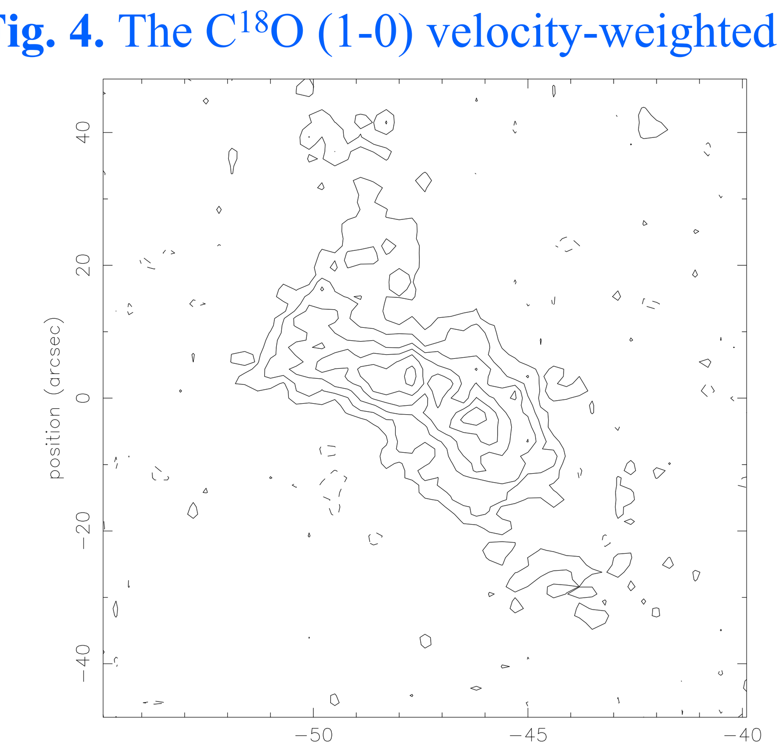

Fig. 5. The position-velocity diagram along the axis at P.A.=47°

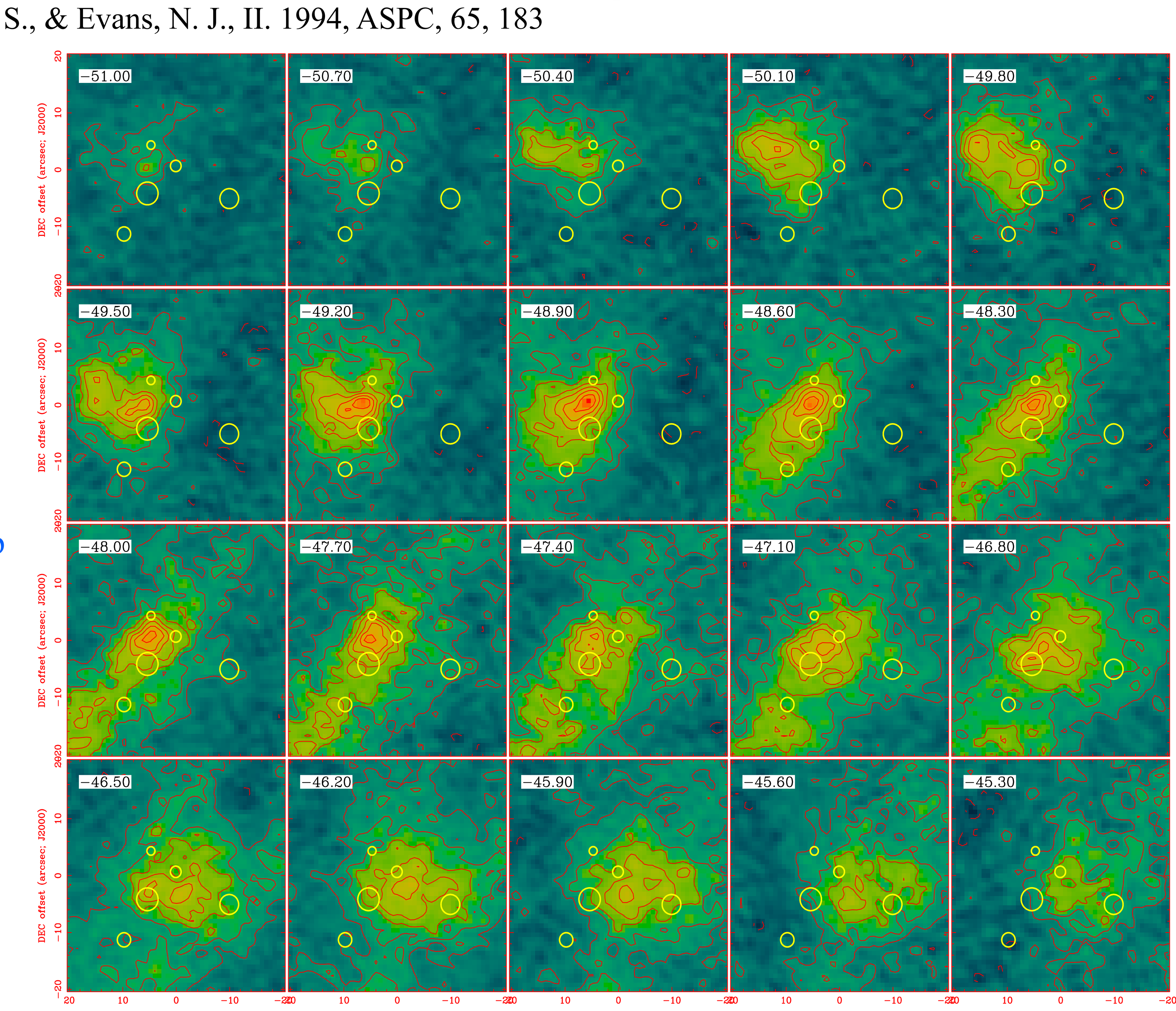

Fig. 3. The $C^{18}O$ (1-0) velocity channel map

Analysis

Infall motions with RATRAN (Hogerheilde & Van der Tak 2000)

In our RATRAN (radiative transfer and molecular excitation) simulation, we model the envelope with 8 concentric spherical shells with a power-law density and velocity distribution (Shu 1977), $n(r) = n_0(r/r_0)^{-2}$ and $v(r) = v_0(r/r_0)^{-0.5}$ with $r_0 = 0.01$ pc (1.3"). The temperature distribution is $T(r) = T_0\ (r/r_0)^{-0.4}$ (Goldreich & Kwan 1974). A fractional abundance of $X(HCO^+) = 1.44 \times 10^{-9}$ is used (Kim et al. 2006). We also estimate an inner radius of 0.01 pc (1.3") and an outer radius 0.27 pc (34") for the envelope. Our preliminary results give $n_0 = 8 \times 10^6\ cm^{-3}$, $v_0 = 2.0\ kms^{-1}$, and a linewidth of 2.3 kms^{-1}. The model spectrum is shown in Fig 1a.

Discussion and Future Work

In RATRAN simulation, we were able to reproduce the general properties of the observed "blue-skewed" line profile. Yet the central dip in our observed spectrum is overall deeper than that in our model spectra. This is due to the lack of a bright continuum source in the models. As for our study of rotation motions, we can estimate that the mass of this infalling envelope within 0.06 pc is about 110 $M_{\odot}$. Our next step is to include the effect of a strong continuum source at the center and to utilize other possible models for the inclusion of rotation motions in our infall envelope.

Reference

Evans, N. J., II 1999, ARA&A, 37, 311
Goldreich, P. & Kwan, J. 1974, ApJ, 189, 441
Harten, R. H. 1976, A&A, 46, 109
Hogerheijde, M. R., & van der Tak, F. F. S. 2000, A&A, 362, 697
Kim, S., Kim, H., Lee, Y., et al. 2006, ApJS, 162, 161
Matsumoto N. et al. 2011, PASJ, 63, 1345
Shu, F. H. 1977, ApJ, 214, 488
Wilson, T. L., Gaume, R. A., & Johnston, K. J. 1993, ApJ, 402, 230
Zhou, S., & Evans, N. J., II. 1994, ASPC, 65, 183